# Threading-the-Needle: Compatibilization of HDPE/iPP Blends with Butadiene-derived Polyolefin Block Copolymers

2 3 4

1

Liyang Shen<sup>a,+</sup>, Gabriela Diaz Gorbea<sup>a,+</sup>, Evan Danielson<sup>a</sup>, Shuquan Cui<sup>b</sup>, Christopher J. Ellison<sup>a,\*</sup>, and Frank S. Bates<sup>a,\*</sup>

5 6

- 7 a Department of Chemical Engineering and Materials Science, University of Minnesota,
- 8 Minneapolis, Minnesota 55455, United States
- 9 b Department of Chemistry, University of Minnesota, Minnesota, Minnesota 55455, United
- 10 States
- 11 + L.S. and G.D.G. contributed equally to this work
- \* To whom correspondence may be addressed. Email: bates001@umn.edu, cellison@umn.edu

13

15

16

17

18

19

20

21

22

23

24

25

26

27

28

29

14 Abstract

Management of the plastic industry is a momentous challenge, one that pits enormous societal benefits against an accumulating reservoir of nearly indestructible waste. A promising strategy for recycling polyethylene (PE) and isotactic polypropylene (iPP), constituting roughly half the plastic produced annually worldwide, is melt blending for reformulation into useful products. Unfortunately, such blends are generally brittle and useless due to phase separation and mechanically weak domain interfaces. Recent studies have shown that addition of small amounts of semicrystalline PE-iPP block copolymers (ca. 1 wt%) to mixtures of these polyolefins results in ductility comparable to the pure materials. However, current methods for producing such additives rely on expensive reagents, prohibitively impacting the cost of recycling these inexpensive commodity plastics. Here we describe an alternative strategy that exploits anionic polymerization of butadiene into block copolymers, with subsequent catalytic hydrogenation, yielding E and X blocks that are individually melt miscible with PE and iPP, where E and X are poly(ethylene-ranethylethylene) random copolymers with 6% and 90% ethylethylene repeat units, respectively. Cooling melt blended mixtures of PE and iPP containing 1 wt% of the triblock copolymer EXE of appropriate molecular weight, results in mechanical properties competitive with the component 1 plastics. Blend toughness is obtained through interfacial topological entanglements of the

2 amorphous X polymer and semicrystalline iPP, along with anchoring of the E blocks through

cocrystallization with the PE homopolymer. Significantly, EXE can be inexpensively produced

using currently practiced industrial scale polymerization methods, offering a practical approach to

recycling the world's top two plastics.

6

7

9

10

11

12

13

14

15

16

3

4

5

## **Significance Statement**

8 Plastic waste constitutes a rapidly growing environmental dilemma, with about half the current

and projected production of these vital materials centered on polyethylene (PE) and isotactic

polypropylene (iPP). Recycling polyolefins is stymied by the technical and financial challenges

associated with separating these materials in waste streams, making melt mixing and reformulation

of the plastics into new products an attractive option. Retention of the essential mechanical

properties in phase separated blends of PE and iPP requires the use of interfacially active block

copolymers. This report exposes an economically viable approach to accomplishing this goal based

on the polymerization and subsequent catalytic hydrogenation of inexpensive butadiene, leading

to block copolymers that can be produced in existing industrial facilities.

17

## Introduction

1

2

3

4

5

6

7

8

9

10

11

12

13

14

15

16

17

18

19

20

21

22

23

Plastics contribute indispensable value to virtually all aspects of modern life, exemplified by: (i) high-density polyethylene (PE) used in artificial hips, bullet proof vests, and natural gas piping<sup>1</sup>; (ii) food packaging of all types<sup>2</sup>; and (iii) modern windmill blades made from thermoset polymer composites<sup>3</sup>. Global production in 2021 of the two largest volume plastics, PE and isotactic polypropylene (iPP), was 107 million metric tons (MMT) and 75.6 MMT, respectively, representing over half of the total synthetic polymer market; the combined output of these polyolefins is estimated to be 230 MMT by 2029.<sup>4,5</sup> These inexpensive and remarkably versatile plastics offer many societal benefits, yet contribute to a rapidly growing reservoir of nearly indestructible waste<sup>6,7</sup>, which ends up in landfills and the environment, including the oceans.<sup>8</sup> Together PE and iPP comprise more than two-thirds of the average discarded plastic waste stream. <sup>9</sup> Several approaches for addressing this crisis are being explored <sup>10–12</sup>, such as chemical upcycling into feedstock chemicals (e.g. hydrogenolysis)<sup>13–15</sup>, and reintroduction of polyolefins into the economy through reprocessing 16-18. However, sorting polyolefin products in a recycle stream by flotation or optical methods is largely ineffective due to similar densities and virtually identical chemical structures (both are saturated hydrocarbons). <sup>19</sup> Combining most PE and *i*PP products for reuse through melt blending results in phase separation leading to brittle and essentially useless materials due to poor interfacial adhesion<sup>20–22</sup>, obviating an otherwise attractive approach to recycling.

Recent advances in organometallic chemistry have afforded access to PE-iPP multiblock copolymers, shown to be remarkably effective at compatibilizing the associated commercial homopolymers at low concentrations (i.e.  $\leq 1$  wt%). Simple melt blending followed by molding at elevated temperatures and cooling to ambient conditions leads to solid specimens with

physical properties comparable to the pristine homopolymer components, e.g. equivalent elastic modulus and high ductility with tensile strain at break  $\omega \approx 300-600\%$ ; unmodified blend specimens containing 70% PE fail at  $\omega < 20\%$ . This strategy is significantly more efficient than competing blend modifiers that rely on commercially available random copolymers such as ethylene-propylene rubber (EPR<sup>25–27</sup> and EPDM<sup>28,29</sup>) or Dow Chemical's INFUSE and INTUNE olefin block copolymers (OBCs), which require larger loadings (i.e. > 5 wt%) to achieve comparable blend toughness. Lin et al.<sup>30,31</sup> report the compatibilization of PE/iPP blends using a series of INFUSE OBCs. Adding 10 wt% OBC enhanced the tensile properties of the blends but did not fully recover the ductility of the neat PE or iPP. Wolff et al.<sup>32</sup> compared the mechanical properties of a HDPE/iPP 30/70 blend compatibilized with INTUNE and INFUSE, and neither OBC produced tensile properties comparable to the neat iPP at 5 wt% loading. However, living block polymerization of ethylene and propylene requires one pyridyl amido hafnium molecular complex per macromolecule, which likely makes this strategy uneconomical. <sup>23,24,33</sup>

The effectiveness of PE-*i*PP multiblock copolymers in recycling polyethylene and polypropylene has been attributed to two factors: (1) thermodynamic compatibility of the two block types with the homologous polyolefins leads to melt state interfacial activity in the phase separated blends; and (2) cocrystallization of the blocks with PE and *i*PP homopolymers binds the two phases together, eliminating interfacial debonding during deformation, the principal mode of failure in the unmodified composites. Here we demonstrate comparable toughening of PE and *i*PP blends after mixing small amounts (ca. 1 wt%) of a poly(ethylene)-*block*-poly(ethylene-*ran*-ethylethylene)-*block*-poly(ethylene) triblock copolymer, denoted EXE, with the same commercial polyolefin homopolymers studied previously. EXE is obtained through anionic polymerization of butadiene followed by catalytic hydrogenation, processes currently practiced on an industrial scale.

- 1 These findings expose a new mechanism of interfacial strengthening, dubbed threading-the-needle,
- which combines topological entanglement of *iPP* melt-compatible and amorphous X center blocks
- 3 with PE cocrystallizable terminal E blocks. This strategy eliminates the need to employ expensive
- 4 organometallic catalysts, thus bringing recycling of polyolefins through blending closer to
- 5 practical reality.

#### Results

6

7

8

10

11

12

13 14

15

16

$$\begin{array}{c} + & Li \\ \hline & & & \\ \hline &$$

Fig. 1. Synthetic scheme for the preparation of EXE triblock copolymer, where the fraction of ethylethylene repeat units in the E blocks (red) is  $x \approx 0.06$  and in the X blocks (blue) is  $y \approx 0.9$ .

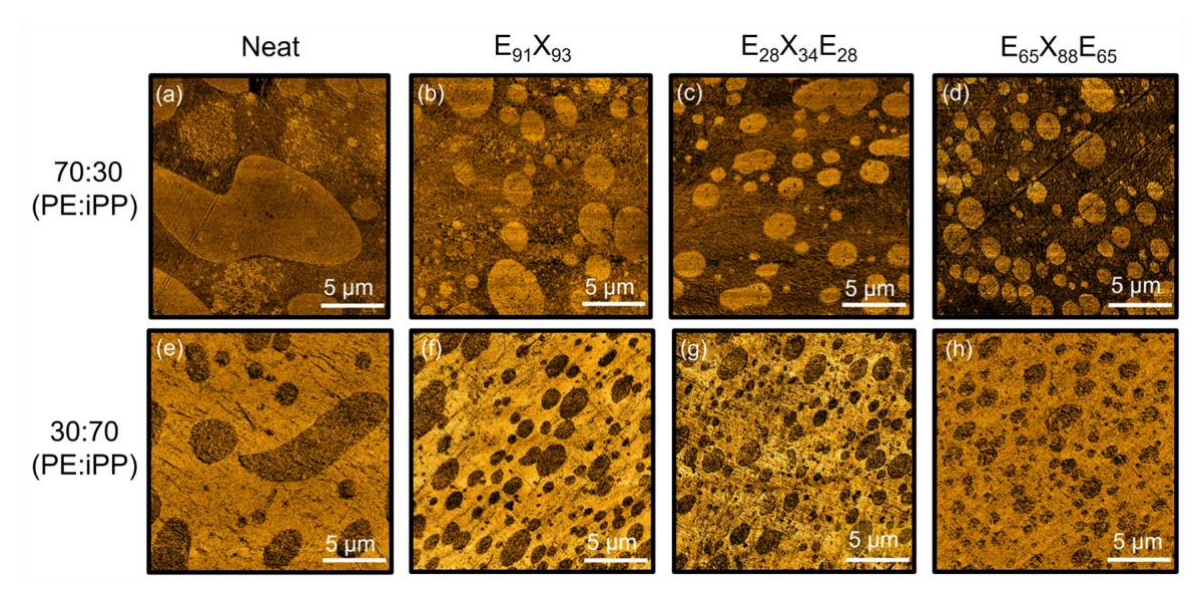
**Table 1** Molecular Characteristics of EX and EXE Block Copolymers

Sample <sup>a</sup>	M₁ (kDa) °	$D \over (M_{ m w}/M_{ m n})$	fx <sup>e</sup>	% ethylethylene in X block	T <sub>g</sub> , X block (°C) <sup>f</sup>	Tm, E block (°C) f
E91X93	184	1.08	50	86	-30	103
E65X88E65 b	176 (218) <sup>d</sup>	1.20	40	90	-28	104
E <sub>28</sub> X <sub>34</sub> E <sub>28</sub> <sup>b</sup>	74 (90) <sup>d</sup>	1.18	38	91	-28	107

<sup>a</sup> Subscripts x and y in E<sub>x</sub> and X<sub>y</sub> indicate number-average molecular weights in kg/mol. <sup>b</sup> Subscripts based on the molecular weight of the polybutadiene diblock copolymer prior to coupling. The molecular weight of the triblock copolymer is calculated based on the molecular weight of the diblock (see *SI Appendix*). <sup>c</sup> Based on SEC using universal calibration with polystyrene standards, <sup>1</sup>H NMR, and corrected for the addition of hydrogen (see *SI Appendix*). <sup>d</sup> Based on the molecular weight of the diblock prior to coupling. The lower molecular weight reflects about 80% coupling efficiency as shown in Fig. S2. <sup>e</sup> Volume fraction of X block based on <sup>1</sup>H NMR, and assuming equal block melt densities. <sup>f</sup> Based on DSC measurements.

1 **Synthesis** The synthetic scheme for producing EXE triblock copolymers is shown in Fig. 1. Initiation of butadiene with sec-butyllithium in cyclohexane at 40 °C leads to a polymer 2 containing 94 mol% 1,4-butadiene and 6 mol% 1,2-butadiene addition, referred to as 1,4-PB. 3 4 Tetrahydrofuran (THF) is added to the living polymer solution at a molar concentration of [THF]: [Li] = 200:1 followed by addition of more butadiene monomer at 20 °C to produce a second 1,4-5 6 PB/1,2-PB statistical copolymer block with ≈ 90% 1,2-PB content, denoted 1,2-PB. Following 7 complete conversion of the monomer to polymer, a stoichiometric amount of 8 dichlorodimethylsilane ([Cl-Si(CH<sub>3</sub>)<sub>2</sub>-Cl]:[Li] = 1:2) is used to couple the living diblock 9 copolymer chains leading to predominately 1,4-PB-block-1,2-PB-block-1,4-PB triblock 10 copolymer. (Alternatively, termination of the living 1,4-PB or 1,4-PB-block-1,2-PB chains with 11 acidic methanol results in homopolymer or diblock copolymer, respectively). Saturation of the 12 block copolymers with hydrogen at 100 °C using a macroporous Pt/SiO<sub>2</sub> catalyst (or various other 13 homogeneous catalysts) generates the desired products, EXE and EX, where the E block contains 14 1.5 ethyl branches per 100 backbone carbon atoms and the X blocks are statistical copolymers 15 with about 90% ethylethylene and 10% ethylene repeat units. (Here we note that polybutadiene 16 can be efficiently saturated using various heterogeneous and homogeneous catalysts, including those associated with large scale industrially practice.<sup>34</sup>) Representative size exclusion 17 18 chromatography (SEC) and proton nuclear magnetic resonance (<sup>1</sup>H NMR) traces of the unsaturated 19 polybutadiene block copolymers are provided in SI Appendix Figs. S1 and S3, respectively. We 20 detect little homopolymer in the specimens (Fig. S1), moreover, any such homopolymer would 21 simply disperse into the PE domain during melt processing and have no influence on the blend 22 properties. The coupling efficiency results in approximately 80 wt% of triblock copolymer as determined using SEC, as shown in SI Appendix Fig. S2, consistent with literature values. 35–37 <sup>1</sup>H 23

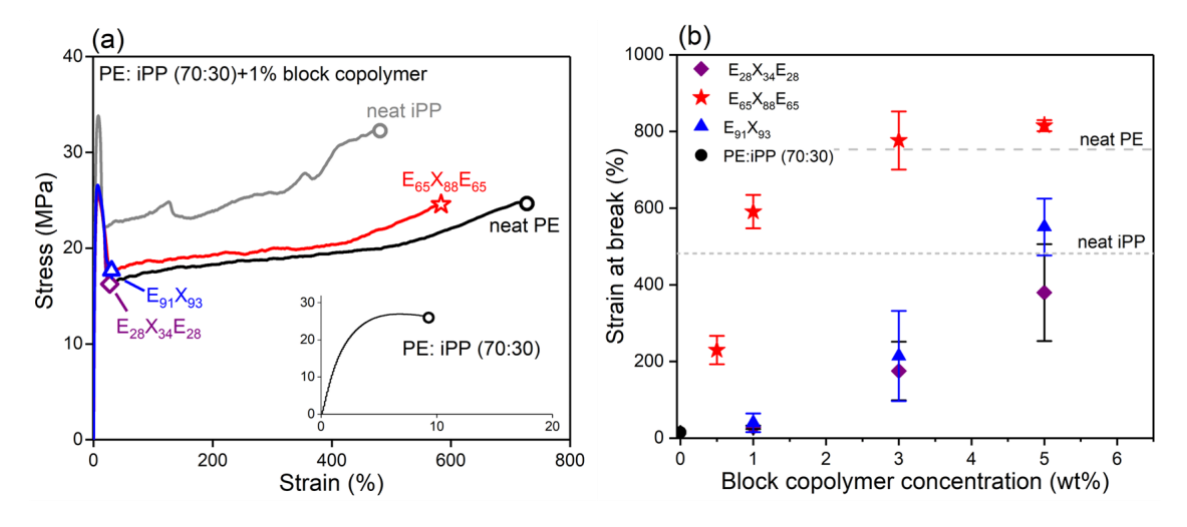
NMR and SEC traces of the saturated products (*SI Appendix* Figs. S4 and S5) demonstrate complete hydrogenation (> 99%) without degradation. The molecular characteristics of the saturated block copolymers are summarized in Table 1. All three block copolymers listed in Table 1 are microphase separated in the melt state up to 240 °C as evidenced through dynamic mechanical spectroscopy measurements (Figs. S7 to S10).



**Fig. 2.** Representative AFM phase images of neat PE/iPP blends (a,e), and blends containing 1 wt%  $E_{91}X_{93}$  (b, f),  $E_{28}X_{34}E_{28}$  (c, g), and  $E_{65}X_{88}E_{65}$  (d,h). The top and bottom rows depict PE:*i*PP compositions of 70:30 and 30:70, respectively. Light and dark domains correspond the *i*PP and PE. Reduction in the domain sizes with the addition of block copolymer is indicative of interfacial activity.

*Blend Morphology* Polymer blends containing commercial high-density polyethylene (HDPE, referred to as PE) and isotactic polypropylene (*i*PP), both provided by the Dow Chemical Co., along with 0.5-5 wt% EXE or EX, were prepared using a recirculating twin screw microcompounder operated at 190 °C followed by molding into 0.5 mm thick films at 180 °C and subsequent cooling (~20 °C/min) to room temperature. Blend morphologies were characterized with atomic force microscopy (AFM) and scanning electron microscopy (SEM). Fig. 2 illustrates representative AFM images obtained from blends of PE and *i*PP containing either 70% or 30%

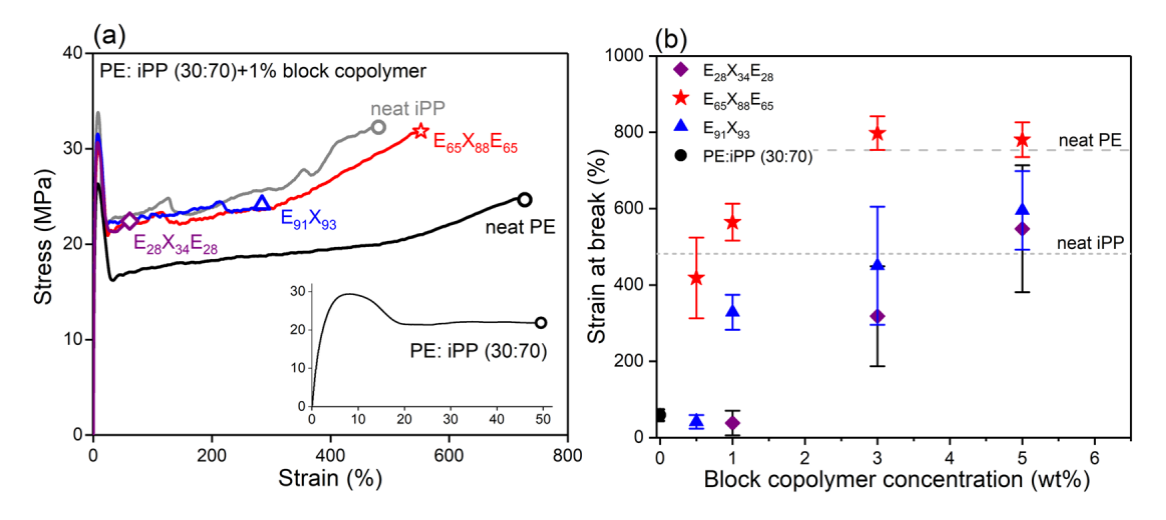
polyethylene (PE:iPP = 70:30 or 30:70, respectively) without (unmodified) and containing 1 wt% of E $_{91}$ X $_{93}$ , E $_{28}$ X $_{34}$ E $_{28}$ , or E $_{65}$ X $_{88}$ E $_{65}$ . Phase contrast is derived primarily from the difference in modulus between the two components, where the softer PE and stiffer iPP materials appear darker and lighter, respectively. Melt mixing results in droplet morphologies, where the block copolymer modified blends consistently show smaller domain sizes and narrower size distributions compared to the neat blends (see *SI Appendix* Figs. S11 and S12). These results evidence localization of block copolymer at the phase separated domain interfaces, which reduces the interfacial tension facilitating droplet breakup during mixing. Minor variations in the domain dimensions between the PE continuous and iPP continuous blends can be attributed to the well-established effects associated with differences in the homopolymer viscosities. <sup>38</sup>



**Fig. 3.** (a) Representative stress-strain curves for neat PE and *i*PP homopolymers, and 70:30 blends containing 1 wt% block copolymer. The inset in (a) shows the stress-strain response of the uncompatibilized blend. (b) Strain at break, *ε*<sub>b</sub>, of compatibilized 70:30 PE:*i*PP blends as a function of block copolymer concentration. Error bars represent one standard deviation.

*Mechanical Properties* Representative stress-strain curves obtained from neat PE and *i*PP homopolymers, and PE:*i*PP (70:30) blends with and without 1 wt% block copolymer, are shown in Fig. 3a. Both homopolymers are tough, exhibiting strains at break of  $\varepsilon_b \approx 450\%$  (*i*PP) and  $\varepsilon_b \approx$ 

750% (PE). Blending these two polyolefins together results in a brittle plastic with  $a_b \approx 10\%$  (inset of Fig. 3a), similar to previously published results. Adding just 1 wt% of the  $E_{65}X_{88}E_{65}$  triblock copolymer leads to full recovery of ductility with  $a_b \approx 600\%$ , a mechanical signature of compatibilization. Substituting the  $E_{28}X_{34}E_{28}$  for  $E_{65}X_{88}E_{65}$  (41% of the higher molecular weight triblock) or replacing the triblock with a relatively high molecular weight diblock ( $E_{91}X_{93}$ ) at the same 1 wt% loading, results in significantly reduced blend toughness ( $a_b < 40\%$ ). Fig. 3b illustrates the role of block copolymer concentration on tensile toughness for the three additives. Considerable ductility ( $a_b > 200\%$ ) is obtained with just 0.5 wt% of  $E_{65}X_{88}E_{65}$ , increasing to about 800% at a concentration of 5 wt%, roughly equivalent to that of pure PE. Both  $E_{28}X_{34}E_{28}$  and  $E_{91}X_{93}$  exhibit modest benefits ( $a_b \approx 200\%$ ) at 3 wt% and about twice this value at 5 wt% loadings.

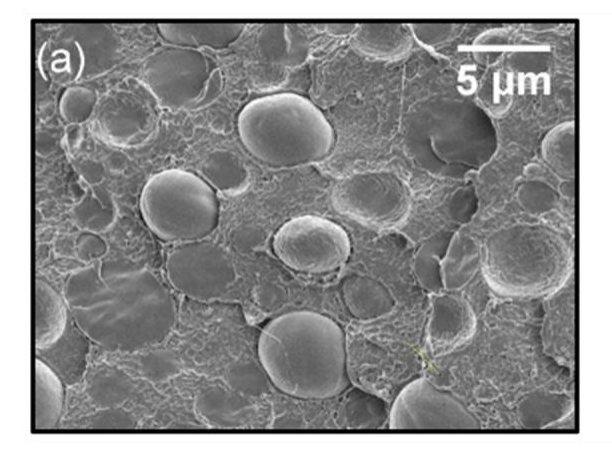


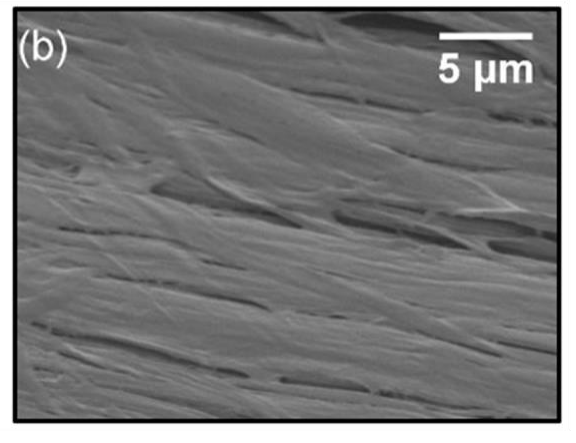
**Fig. 4.** (a) Representative stress-strain curves for neat PE and iPP homopolymers, and 30:70 blends containing 1 wt % block copolymer. The inset in (a) shows the stress-strain response of the uncompatibilized blend. (b) Strain at break,  $\varepsilon_0$ , of compatibilized 30:70 PE:iPP blends as a function of block copolymer concentration. Error bars represent one standard deviation.

Fig. 4a summarizes the mechanical properties of *i*PP continuous (30:70 PE:*i*PP) blends with 1 wt% of each of the three block copolymers, along with the uncompatibilized mixture. Here again, the unmodified mixture exhibits a reduced ductility ( $\varepsilon_b \approx 50\%$ ) relative to the pure polyolefins; we

attribute the increase in  $\omega$  compared to the unmodified 70:30 blend (Fig. 3a) to the dispersion of the more compliant PE as particles in a stiffer *i*PP matrix. And as before, adding just 1 wt% of the E<sub>65</sub>X<sub>88</sub>E<sub>65</sub> triblock copolymer results in a strain at break ( $\omega \approx 550\%$ ) intermediate to the pure homopolymers. As shown in Fig. 4b, the dependence of the strain at break on block copolymer concentration for the 30:70 blends resembles what appears in Fig. 3b, with a couple of notable exceptions: diblock copolymer E<sub>91</sub>X<sub>93</sub> promotes significantly greater toughness in the 30:70 blend at a concentration of 1 wt%, and E<sub>65</sub>X<sub>88</sub>E<sub>65</sub> affords nearly twice the strain at break at 0.5 wt% as was obtained with the 70:30 PE:*i*PP mixture.

Overall, the most striking discovery of this work is that triblock copolymer E<sub>65</sub>X<sub>88</sub>E<sub>65</sub> performs as well in toughening the same PE:*i*PP blends as the fully semicrystalline PP<sub>60</sub>PE<sub>80</sub>PP<sub>75</sub>PE<sub>90</sub> tetrablock copolymer reported earlier.<sup>23</sup>





**Fig. 5.** SEM images obtained from cryo-fractured cross-sections of (a) PE:*i*PP (70:30) blend following failure in tension at  $\varepsilon_b \approx 10$  %, and (b) PE:*i*PP (70:30) blend containing 1 wt% E<sub>65</sub>X<sub>88</sub>E<sub>65</sub> after failure at  $\varepsilon_b \approx 600$  %.

Brittle fracture in uncompatibilized polyolefin blends has been attributed to interfacial failure when such composites are subjected to large deformations. As demonstrated by the SEM image in Fig. 5a, *i*PP particles appear to be cleanly separated from the PE matrix along the fracture

surface in a failed 70:30 PE:*i*PP blend specimen ( $\varepsilon_b \approx 10\%$ ). In sharp contrast, the addition of 1 wt% E<sub>65</sub>X<sub>88</sub>E<sub>65</sub> completely suppresses interfacial failure during tensile deformation resulting in drawing of both the matrix and particle domains without delamination up to the point of fracture ( $\varepsilon_b \approx 600\%$ ) as seen in Fig. 5b.

Crystallization The physical properties of semicrystalline polyolefins are intimately connected with the detailed molecular configurations associated with chain-folded crystalline morphologies. These in turn are determined by several factors, including the number of chain defects (e.g., the fraction of branches in PE or stereochemical irregularity in iPP) and the crystallization temperature, which is influenced by the rate of cooling from the melt state. The latter point was evaluated with the PE and iPP homopolymers by preparing rapidly (20 °C/min) and slowly (1 °C/min) cooled specimens, followed by tensile testing. The PE material exhibited a modest reduction in strain at break at the slower cooling rate (from  $\omega \approx 750\%$  to  $\omega \approx 550\%$ ) (SI Appendix Fig. S19a). However, when cooled at 1 °C/min, the iPP plastic became brittle, failing at  $\omega \approx 10\%$  in contrast to  $\omega \approx 500\%$  when cooled at 20 °C/min (SI Appendix Fig. S19b). (Here we note that most commercial processing involves relatively rapid cooling rates, dT/dt > 20 °C/min). We conducted a series of differential scanning calorimetry (DSC) experiments to establish the crystallization behavior of the PE and iPP homopolymers as a function of cooling rate.

As illustrated in *SI Appendix* Fig. S20, both homopolymers crystallize ( $T_c$ ) and melt ( $T_m$ ) at slightly lower temperatures when cooled more rapidly: (i) dT/dt = 1 °C/min,  $T_{c,PE} = 119.9$  °C,  $T_{m,PE} = 133.1$  °C, and  $T_{c,iPP} = 128.5$  °C,  $T_{m,iPP} = 164.2$  °C; (ii) dT/dt = 20 °C/min,  $T_{c,PE} = 117.0$  °C,  $T_{m,PE} = 130.2$  °C, and  $T_{c,iPP} = 117.8$  °C,  $T_{m,iPP} = 161.4$  °C. These trends are also reflected in the percent crystallinity: 63% versus 60% for PE and 58% versus 52% for iPP at the slower and faster

cooling rates, respectively. We attribute the ductile to brittle transition associated with *i*PP as the cooling rate is lowered to the increased crystallinity.

1

2

3

4

5

6

7

8

9

10

11

12

13

14

15

16

17

18

19

20

21

22

23

In the Discussion section (see below), we propose a molecular scale mechanism to explain the extraordinary toughness imparted to PE:iPP blends by the addition of small amounts of the E<sub>65</sub>X<sub>88</sub>E<sub>65</sub> triblock copolymer. A key aspect of this hypothesis relies on cocrystallization of the E blocks with the PE homopolymer in the vicinity of the interfacial region between the phase separated domains. In order to probe such cocrystallization, two 1,4-PB homopolymers were synthesized and hydrogenated as described in the SI Appendix. We refer to these as E<sub>35</sub> and E<sub>65</sub> where the molecular weights were chosen to be similar to the E blocks in the two triblock copolymers (Table 1). DSC measurements show that these polymers have about 36% crystallinity with melting temperatures of  $T_{m,E} = 108-110$  °C, following cooling from the melt at 20 °C/min, i.e., slightly higher than the melting temperatures of the E blocks in the pure block copolymers (Table 1). The difference in percent crystallinity and melting temperature  $T_{m.PE}$  -  $T_{m.E} \approx 21$  °C is attributable to the 1.5 ethyl branches per 100 backbone carbon atoms in the E polymer, which can result in segregation during melt crystallization in mixtures with the PE homopolymer. DSC experiments with blends of E<sub>35</sub> and E<sub>65</sub> containing PE demonstrate that these polymers largely cocrystallize when cooled from the melt at 20 °C/min, as evidenced by a depression of the principle melting temperature to  $T_m = 126-128$  °C, and reduction in the percent crystallinity to 48%-50%, in mixtures containing 50% of either E polymer; a minority fraction (< 50%) of E segregates during solidification as indicated by a broad second melting endotherm at 108-110 °C in these blends (SI Appendix Fig. S17). Mixtures containing 25% E and 75% PE exhibit almost no evidence of segregation after crystallization. Cooling these mixtures slowly (1 °C/min) somewhat increases segregation between E and PE during crystallization as evidenced by a slightly higher principal peak melting temperature (129-130 °C) and a more distinct lower melting temperature (≈ 108 °C) endotherm in the 50/50 PE/E mixtures (*SI Appendix* Fig. S18). Wignall et al. reported that slowly cooling induces the formation of separate crystalline phases in HDPE/LDPE blends based on small-angle neutron and X-ray scattering and DSC measurements.<sup>39</sup> These experiments show that, to a considerable extent, E<sub>35</sub> and E<sub>65</sub> cocrystallize with PE when cooled rapidly from the mixed melt state, with some degree of segregation in the solid state after slow cooling.

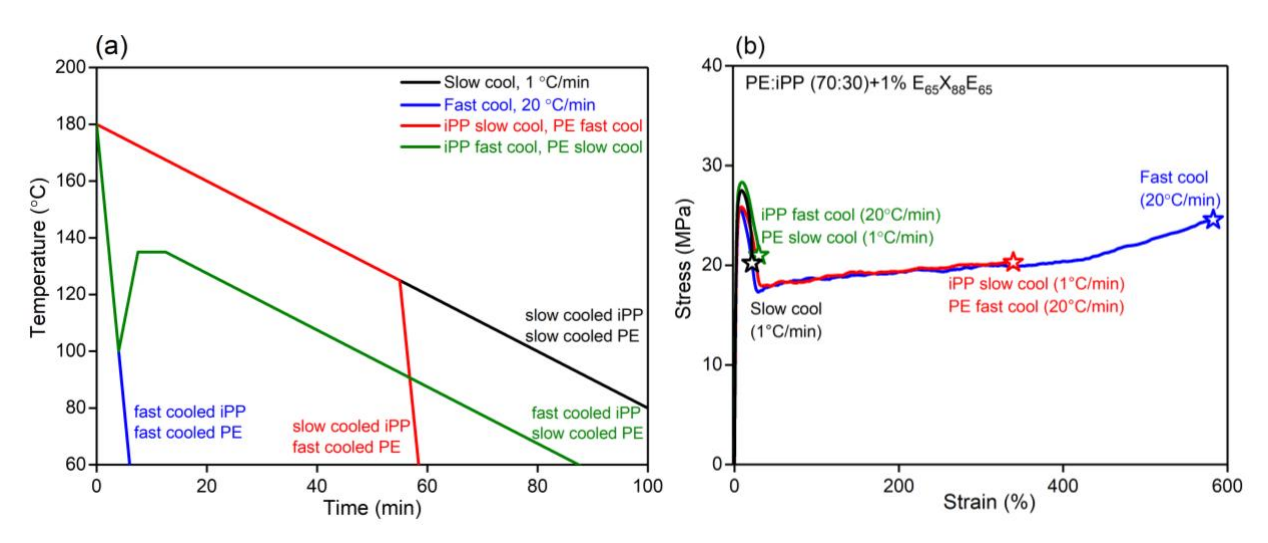


**Fig. 6.** (a) Schematic illustration of four thermal processing strategies, where slow cool  $\cong$  1 °C/min and fast cool  $\cong$  20 °C/min. 1) Slow cool *i*PP/slow cool PE from 180 to 30 °C (red/black lines). 2) Fast cool *i*PP/fast cool PE from 180 to 30 °C (green/blue lines). 3) Slow cool *i*PP/fast cool PE; slow cool from 180 to 125 °C (red line) followed by fast cool from 125 to 30 °C (red line). 4) Fast cool *i*PP/slow cool PE; fast cool from 180 to 100 °C (green line) followed by heating from 100 to 135 at 10 °C/min (green line), isothermal annealing for 10 min at 135 °C (green line) then slow cooling from 135 to 30 °C. (b) The representative stress-strain curves obtained from PE: iPP (70:30) blends with 1 wt. %  $E_{65}X_{88}E_{65}$  following different cooling recipes from the melt state.

We performed analogous solidification experiments with the 70:30 PE:iPP blend containing 1 wt% E<sub>65</sub>X<sub>88</sub>E<sub>65</sub>, guided by the thermal behavior determined for the two homopolymers. Fig. 6 highlights the mechanical properties obtained following 4 different cooling and heating procedures that are summarized in *SI Appendix* Fig. S21. A tough blend ( $\varepsilon_b \approx 600\%$ ) is obtained in the limit of fast cooling (20 °C/min) from the melt (180 °C) as described earlier. Reducing the cooling rate to 1 °C/min has a profound impact on the product, decreasing the strain

at break to  $a_0 \approx 25\%$ . A third thermal history involved cooling from 180 °C at 1 °C/min (slow cool) to 125 °C followed by cooling at 20 °C/min (fast cool) to room temperature, designated "iPP slow cool/PE fast cool" in Fig. 6. This protocol, designed to produce crystalline iPP particles dispersed in a PE melt at 125 °C, with subsequent crystallization of PE (and E) while cooling slowly, results in a tough material, albeit with a somewhat reduced strain at break,  $a_0 \approx 350\%$ . In a fourth procedure, the entire blend was solidified by fast cooling from 180 °C to 100 °C (i.e. well below the crystallization temperature of both PE and iPP), then was heated to 135 °C for 5 minutes (leaving fast cooled crystalline iPP dispersed in a PE melt), followed by slow cooling to room temperature. This process, referred to as "iPP fast cool/PE slow cool" in Fig. 6, results in a relatively brittle plastic with  $a_0 \approx 30\%$ . These surprisingly different materials are discussed further in the following section in the context of the "threading-the-needle" mechanism.

## **Discussion**

Addition of a small amount (ca. 1 wt%) of an appropriately prepared EXE triblock copolymer to mixtures of commercially available polyethylene and polypropylene leads to remarkably tough materials, offering a promising approach to recycling these leading plastics. At first blush, this finding is surprising because the X block, which is an amorphous polymer with a glass transition temperature  $T_{g,X} = -30$  °C, cannot cocrystallize with *i*PP. The results presented in the previous section offer important clues as to the mechanism responsible for this intriguing and enabling behavior.

Polyolefin thermodynamics involves purely dispersive van der Waals interactions, hence there is little if any heat of mixing associated with PE and *i*PP melt blends; note that the densities of these chemical isomers in the melt state are nearly identical. Previous theoretical and experimental research has attributed the phase separation of polyolefins to the excess entropy of

mixing associated with differences in the conformational states of saturated hydrocarbon polymers with differing branch types and compositions. According to the conformational asymmetry theory proposed by Bates and Fredrickson<sup>40–42</sup>, miscibility between different polyolefins can be obtained by matching the associated statistical segment lengths at a common segment volume. Random copolymers of ethylene and ethylethylene, containing about 90% of the branched repeat units, denoted X, are well-established to be melt-miscible with iPP (i.e. the Flory-Huggins interaction parameter  $\chi \approx 0$ ) owing to matched statistical segment lengths defined at a common segment volume.<sup>43</sup> Following earlier work by Chaffin et al.<sup>44</sup>, we designed the EXE and EX block copolymers with this in mind. A key factor in applying these compounds to compatibilization of PE and iPP is the segregation of the E and X blocks, which was verified using dynamic mechanical spectroscopy (DMS). Both pure EXE triblocks and the EX diblock display non-terminal low frequency elastic (G') and dynamic (G'') moduli (SI Appendix Figs. S7 to S10) indicative of microphase separation up to 240 °C. Transport of the block copolymers to the interface between the phase separated PE and iPP domains during melt blending is therefore driven by thermodynamic compatibility of E and PE, and X and iPP.

1

2

3

4

5

6

7

8

9

10

11

12

13

14

15

16

17

18

19

20

21

22

23

Interfacial activity of the EXE and EX block copolymers serves two purposes: (1) it reduces the interfacial tension between PE and *i*PP in the melt state, similar to the behavior of a surfactant in contact with water and oil; and (2) the localization of block copolymers at domain interfaces provides varying degrees of adhesion between the solid (semicrystalline) domains. Reduced interfacial tension is evident in the reduction in domain sizes relative to the unmodified mixtures apparent in the AFM images found in Fig. 2; well-established theory and experiments anticipate this tradeoff between particle size and interfacial tension under the influence of shearing and extensional flows in the two-phase liquid systems.<sup>45,46</sup> To a reasonable approximation, diblock

and triblock copolymers should function similarly in this respect, where competing factors set the optimal molecular weight M; increasing M leads to enhanced steric stabilization but promotes micelle formation, while reducing M ultimately results in miscibility of the block copolymer with the homopolymers. This aspect of EXE and EX compatibilization of PE and iPP warrants additional research. Here we focus on interfacial adhesion, which is responsible for achieving tough blends.

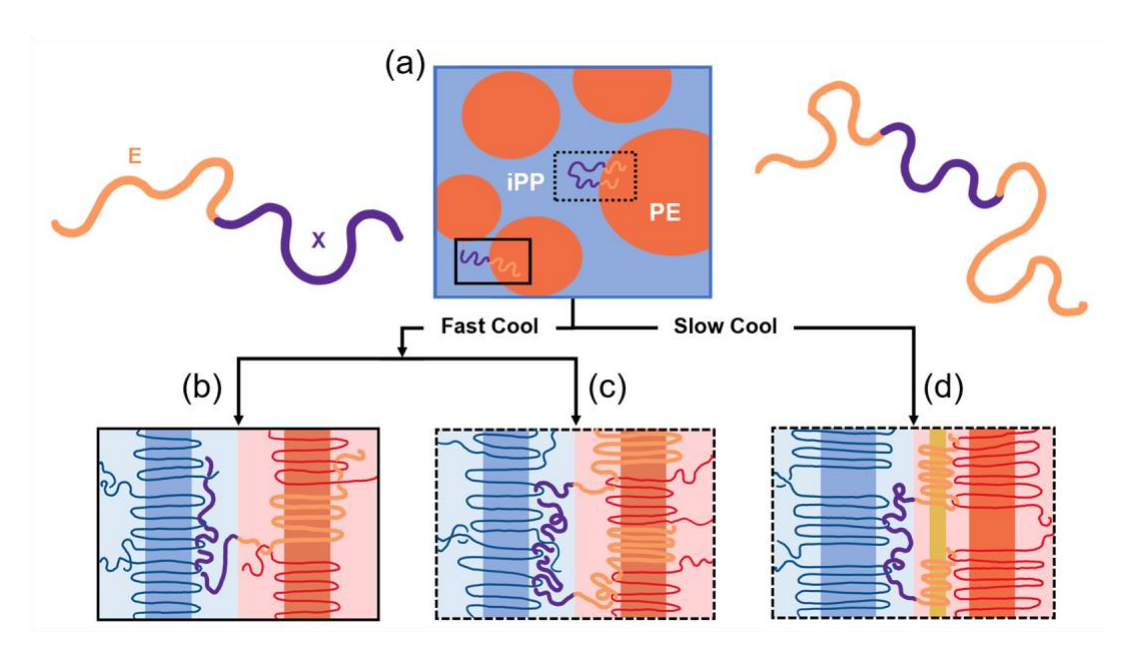


**Fig. 7.** Schematic illustration of proposed mechanisms for block copolymer interfacial behavior in the (a) melt state, and (b-d) solid state. Fast cooling from the melt results in cocrystallization of E and PE, and entanglement of X with the amorphous portion of semicrystalline *i*PP (b,c). A triblock architecture leads to topologically entrained X blocks and high interfacial strength (c). Diblocks present entangled but unconstrained X chains that can disengage from the interface under stress (b). Slow cooling (d) results in semicrystalline E blocks segregated from the PE morphology leading to poor interfacial strength.

EXE triblock and EX diblock copolymers will be configured at the domain interfaces as sketched in Fig. 7a. For the triblock molecular architecture, the X block will form a loop that extends into the liquid *i*PP domain. Assuming Gaussian statistics, the radius of gyration of a flexible polymer is  $R_g = b(N/6)^{1/2}$ , where N is the degree of polymerization and b is the statistical segment length.<sup>41,40</sup> For the X block (and *i*PP based on a 4-carbon repeat unit),  $b_X = b_{iPP} = 0.58$ 

nm<sup>43</sup>, hence the X loop will project roughly  $D = 2R_g$  into the iPP domain; for E<sub>65</sub>X<sub>88</sub>E<sub>65</sub> and  $E_{28}X_{34}E_{28}$ ,  $D_X \approx 19$  nm and 12 nm, respectively. Similarly, the E blocks will project into the PE melt roughly  $D_E \approx 22$  nm and 15 nm, respectively, based on  $b_E = 0.80$  nm (also with a 4-carbon repeat unit). 40,41 Once formed, iPP chains will rapidly penetrate ("thread") the X loop ("needle") in order to maintain constant density, creating a state of entanglement with the homopolymer. (For the iPP melt considered here, the melt molecular diffusion (reptation) time is  $\tau_r < 1$  s). Estimating the X loop volume as  $V_{\rm X} = (4/3)\pi R_{\rm g}^3 = 3.1 \times 10^3 \text{ nm}^3$  with a melt density of  $\rho = 0.9 \text{ g/cm}^3$  yields roughly 10-20 iPP chains within a loop volume for  $E_{65}X_{88}E_{65}$ , based on  $M_{n, iPP} = 1 \times 10^5$  g/mol and assuming the relevant metric is the number average molecular weight. M<sub>n</sub> provides a conservative estimate of the "needle" size. The X blocks are relatively narrow in dispersity so that this distinction is not very important. More significant are the molecular weights and dispersity of the iPP chains in estimating how many of these polymers are entrained in a "needle". We believe the most relevant molecular weight for this purpose is  $M_n$ , as we calculate the number of iPP polymers contained in an X block coil volume. (Clearly these are crude calculations intended to provide a qualitative sense of the proposed mechanism). Since the entanglement molecular weight for polypropylene (and the X blocks) is  $M_e = 6,300 \text{ g/mol}^{49}$ , the homopolymer chains associated with the X loop will be fully entangled. Maintaining the entropically favorable Gaussian coil configuration necessitates penetration of many iPP chains within the associated coil volume. Upon cooling, nucleation and growth of a chain-folded semicrystalline morphology will require local separation of the iPP and X chains, since the latter cannot crystallize. We speculate that the X loops will be entrained by the loops and bridging portions of the amorphous part of the semicrystalline iPP structure, creating topological constraints that bind the E<sub>65</sub>X<sub>88</sub>E<sub>65</sub> triblock copolymer to the iPP domain (see Figs. 7c and 7d). An EX diblock architecture does not afford

1

2

3

4

5

6

7

8

9

10

11

12

13

14

15

16

17

18

19

20

21

22

23

the same type of entrainment since the X block is immobilized only at one end (i.e., the EX block junction in Fig. 7b) and can escape confinement by wiggling out of the *i*PP entanglements in response to an applied load. However, the diblock will be interfacially active as evidenced by the reduction in domain size shown for the blends containing E<sub>91</sub>X<sub>93</sub> (Figure 2b and 2f). Such interfacial activity will not interfere with the "threading the needle" mechanism associated with

In order to support a stress across the interface, the E blocks also must be bound to the semicrystalline PE domains. Here, we invoke cocrystallization of E and PE, shown above to

the EXE triblock copolymer containing minor amounts of uncoupled diblock copolymer.

occur in blends of the two homopolymers. We speculate that upon rapid cooling a fraction of the

actual mixing of crystalline E and PE stems within common lamellae (Figs. 7b and 7c) or could

E blocks are immobilized through crystallization with the homopolymer. This may involve

result from entrained chain folded loops and bridges between separate crystalline E lamellae and

PE lamellae. What is essential is that a critical fraction of the E blocks are fixed within the PE

domain in order to withstand the forces created at the domain interface during deformation.

The new and most essential feature of the proposed toughening mechanism is that iPP chains "thread-the-needle" formed by the looping X block in the melt state, which becomes topologically trapped upon crystallization of the homopolymer. Anchoring of the E blocks then results in interfacial adhesion. Support for this hypothesis is provided by the experimental results, especially in the limit of low concentrations of block copolymer ( $\leq 1 \text{ wt}\%$ ).

Here we focus on the findings shown in Fig. 6. Superior ductility ( $\varepsilon_b > 300\%$ ) was obtained when PE crystallization occurred under fast cooling conditions, regardless of whether the *i*PP was cooled quickly or slowly. This implies that the threading-the-needle mechanism is not rate dependent. Disengagement of *i*PP during crystallization could occur if folding individual

chains into growing lamellae drew them out of the X loop. However, this would require collapse

of the X loop, which would be entropically costly. We believe that iPP crystallization captures

the X loop in multiple chain-folded and bridging portions of the amorphous region of the

semicrystalline iPP, creating topological crosslinks that stitch the block copolymer to the solid

iPP domain. We anticipate that this mechanism will be operative at considerably lower EXE

molecular weights (see below). However, the E block must be considered as well.

Fig. 6 also reveals that slowly cooling the blends leads to poor ductility. Most tellingly, fast cooling to 100 °C, with crystallization of PE and iPP, followed by melting of the PE (but not the iPP), and then slow crystallization of PE renders a material with  $a_0 \approx 30\%$ , which is almost indistinguishable from blends cooled continuously from 180 °C to room temperature at ~1 °C/min. Clearly, the critical step of E and PE cocrystallization near the domain interface is rate dependent. So As mentioned previously, the extent of cocrystallization between E and PE will be smaller with slow cooling compared to fast cooling from the mixed melt state. Moreover, there appears to be an E block molecular weight dependence. We believe the poor performance of  $E_{28}X_{34}E_{28}$  at low concentrations (Figs. 3 and 4) is due to the reduction from 65 kDa to 28 kDa in the E block molecular weight. These results point to the need to better understand how E and PE engage during crystallization in the vicinity of the domain interfaces.

Overall, the interfacial activity of the EXE triblock is not dependent on the blend composition, i.e. 70:30 PE:iPP versus 30:70 PE:iPP, in both limits acting as a macromolecular surfactant that lowers the interfacial tension while mechanically coupling the two domains through cocrystallization of E and PE, and topological entanglement of X and iPP. The curious behavior of the E<sub>91</sub>X<sub>93</sub> diblock copolymer in the 30:70 PE:iPP blends (Fig. 4) warrants an additional comment. At 1 wt% loading, the fast-cooled mixture exhibits  $a_0 \approx 325\%$  yet this block copolymer

imparts no added toughness beyond the pure homopolymer blend at 0.5 wt%. We suspect this reflects an increased E block molecular weight, combined with the role played by embedding lower modulus PE particles in a stiffer *i*PP matrix, clearly reflected in the unmodified mixture (inset of Fig. 4a). Presumably, interfacial failure occurs through retraction and delamination of the X blocks,

which are probably highly entangled in the amorphous region of the semicrystalline *iPP* domain.

5

6

7

8

9

10

11

12

13

14

15

16

17

18

19

20

21

22

23

Finally, we reflect on the "threading-the-needle" concept in the light of a recent report of remarkable toughness obtained by adding low concentrations of dihydroxy polyethylene (HO-PE-OH) to blends of PE and poly(ethylene terephthalate) (PET).<sup>51</sup> Mixing just 0.5 wt% of HO-PE-OH with molecular weights ranging from 1 to 20 kDa to a 80:20 PET:PE blend and melt processing at 270 °C for 5 minutes produced composites with  $\varepsilon_b \approx 300\%$ ; the unmodified blends were characterized by  $\varepsilon_b < 50\%$ . This processing procedure drives the formation of PET-PE-PET triblock copolymers through transesterification at the interface between the two homopolymers. Ostensibly, this finding seems analogous to what is reported here. However, the underlying "hookand-clasp" mechanism for PET:PE blends is decidedly different than "threading-the-needle". Facile reaction of a terminal HO-PE-OH hydroxyl group with a PET chain generates a diblock copolymer that is "hooked" to the narrow (< 1 nm) interface associated with the strongly phase separated blend. Proximity of the hydroxyl moiety of the resulting PET-PE-OH diblock to additional PET at the interface facilitates a second transesterification reaction leading to a PET-PE-PET triblock copolymer. The resulting "clasping" process captures PE homopolymer chains, and subsequent crystallization of PE and PET upon cooling provides interfacial adhesion. A  $M_n$  = 1 kDa PE chain will have  $V_{PE} \approx 15 \text{ nm}^3$  with roughly 85% of the space available for "clasping" high molecular weight PE homopolymer. Unlike "threading-the-needle," the "hook-and-clasp" mechanism does not require transporting block copolymer to the interface, nor diffusion of PE

- 1 homopolymer; the "clasping" step is driven by the transesterification reaction, greatly enhanced
- 2 by proximity to the interface created by diblock formation. As a consequence, even highly
- 3 compositionally asymmetric triblocks, can efficiently compatibilize PE and PET; preformed PET-
- 4 PE-PET triblock copolymer would not be expected to be as effective. 52

## Conclusion

Repurposing polyethylene (PE) and polypropylene (iPP) through blending requires economically tractable approaches to combining these plastics without sacrificing mechanical properties. We have demonstrated that adding only 1 wt% of EXE triblock copolymers, containing PE and iPP melt miscible E and X blocks, generates ductile blends with a strain at break of  $\varepsilon_0 \approx 600\%$ . The synthetic methods for obtaining this relatively inexpensive block copolymer, anionic polymerization of butadiene followed by catalytic hydrogenation, are currently practiced on an industrial scale. Mechanically superior blends result from interfacial localization of the EXE triblock copolymer during melt mixing, which leads to X chains that are topologically entrained with semicrystalline iPP and E blocks that cocrystallize with the PE homopolymer upon rapid cooling. This new strategy brings the possibility of recycling PE and iPP through blending and reuse closer to feasibility.

## **Materials and Methods**

**Materials.** Homopolymers iPP (H314-02Z,  $M_n = 100 \text{ kg/mol}$ , D = 4.1, MFI = 2.0 g/10 min at 230 °C with 2.16 kg) and HDPE (DMDA-8904,  $M_n = 22 \text{ kg/mol}$ , D = 3.8, MFI = 4.4 g/10 min at 190 °C with 2.16 kg) were both obtained from the Dow Chemical Company. A series of E-X block copolymers were synthesized using sequential anionic polymerization followed by catalytic hydrogenation; detailed descriptions of the procedures have been reported previously. Significant Cyclohexane (HPLC, Fisher Scientific) and tetrahydrofuran (THF) (HPLC, Fisher Scientific) were

purified by passing through activated alumina columns. Butadiene ( $\geq 99\%$ , Sigma-Aldrich) was twice distilled from n-butyllithium (2.5M in hexanes, Sigma-Aldrich). Cyclohexane was first added to the reactor under an argon atmosphere, followed by sec-butyllithium (sBuLi, 1.4M in cyclohexanes, Sigma-Aldrich) and butadiene, which was allowed to react for 8 h at 40 °C. An aliquot of the living polymer was taken to determine the average molecular weight and dispersity. Then the reactor was cooled to 20 °C, and THF was added at a concentration of [THF]:[Li] = 200:1, followed by additional butadiene. After an additional 8 h, an aliquot of the diblock was removed from the reactor for analysis, and a stoichiometric amount of dimethyldichlorosilane ( $\geq 99.5\%$ , Sigma-Aldrich) was added ([C1]:[Li] = 1:1) and allowed to react for 3 days at room temperature. Polybutadiene homopolymers and diblock copolymers were prepared by terminating living polymers following the first and second stages using degassed methanol. The product was precipitated in cold methanol and dried under vacuum at 40 °C to constant weight. Polybutadiene (PB) polymers were dissolved in isooctane (≥ 99%, Fisher Scientific) at a concentration of 5 g/L and hydrogenated to E homopolymers, EX diblock, and EXE triblock copolymers, in a high-pressure reactor operated at 100 °C with 500 psi of H<sub>2</sub> over a SiO<sub>2</sub> supported Pt catalyst (1:5 catalyst-to-polymer (w/w)) for 24 h.<sup>54</sup> Catalyst was removed by hot filtration and the product was precipitated in cold methanol and dried under vacuum at 100 °C to constant weight. The molecular weight and dispersity of the PB compounds were determined using room temperature size exclusion chromatography (SEC) at a concentration of 3-5 mg/mL with THF as the mobile phase and calibrated with polystyrene standards. The eluent flow rate is 1 mL/min, and the sample injection volume is 100 µL. The Mark-Houwink parameters used for the universal calibration are  $K_{PB} = 2.52 \times 10^{-2} \text{ mL/g}$ ,  $\alpha_{PB} = 0.727$ ,  $K_{PS} = 8.63 \times 10^{-3} \text{ mL/g}$ , and  $\alpha_{PS} = 0.736$ . The composition of the 1,4-PB and 1,2-PB blocks were determined by <sup>1</sup>H NMR spectra obtained

1

2

3

4

5

6

7

8

9

10

11

12

13

14

15

16

17

18

19

20

21

22

23

from 10% (w/w) CDCl<sub>3</sub> solutions at 30 °C using a Bruker HD500 NMR spectrometer. The polybutadiene precursors and the hydrogenated products were examined by high-temperature SEC in trichlorobenzene at 135 °C using an Agilent PL-220 instrument equipped with a refractive index detector to confirm a lack of chain degradation, and <sup>1</sup>H NMR spectroscopy was performed with a Bruker HD500 instrument at 90 °C using deuterated toluene solutions to establish the extent of polymer saturation.

Blend Preparation and Tensile Test. Blends of PE, iPP, and 0.5-5 wt% block copolymers (weight fraction based on the weight of neat PE/iPP blends) were prepared using a recirculating 5 mL DSM Xplore twin-screw microcompounder, with mixing for 8 min at 130 rpm at 190 °C. The blended materials were molded into 0.5 mm thick films at 180 °C employing a pressure of 4 MPa for 5 min with a Carver hot press. Unless otherwise stated, cooling water was used for quenching (~20 °C/min). Dumbbell-shaped tensile bars were prepared with a die cutter (ASTM D1708, 5 mm gauge width, 22 mm gauge length). All tensile tests were conducted at room temperature (22 °C) using an Instron 5966 Universal Testing System operated at a crosshead speed of 22 mm/min (100%/min strain rate).

**Atomic Force Microscopy.** The morphology of neat and compatibilized PE:*i*PP blends were imaged using atomic force microscopy in dynamic mode (AFM; Bruker Nanoscope V Multimode 8, Digital Instruments Santa Barbara, CA open-loop system). Smooth imaging surfaces were obtained on pressed and annealed films using a cryo-ultramicrotome (Leica UC6) operated at -120 °C, first using a glass knife to create a cutting face, followed by sectioning of 500 nm thick slices with a diamond knife (Diatome), which were mounted on a silicon wafer. Samples were scanned in the repulsive regime using an n-type silicon tip cantilever (resonant frequency = 166 Hz, spring constant = 2 N/m, and radius = 8 nm). Captured images were processed using Gwyddion

2.56 open-source software to level the data, align rows, correct scarring, and adjust the contrast via histogram. Details regarding data handling are provided in the *SI Appendix*.

**Fractography.** Dogbone tensile specimens were cryo-fractured in liquid nitrogen, and the resulting cross sections were examined using a JEOL 6500 field emission SEM with 2 kV accelerating voltage and approximately 10 mm working distance. Specimens were affixed with carbon tape to a 90-degree pin stub mount and sputter coated with a 5 nm thick platinum conducting layer before imaging.

**Thermal Analysis.** Glass transition, melting and crystallization temperatures were determined using differential scanning calorimetry (DSC). 5–10 mg of sample was sealed in an aluminum pan and loaded in a TA Q1000 DSC instrument under a nitrogen atmosphere at gas flow rate 50 mL/min.

**Rheology.** Bulk rheological data were acquired for the three saturated block copolymers (E<sub>91</sub>X<sub>93</sub>, E<sub>28</sub>X<sub>34</sub>E<sub>28</sub>, and E<sub>65</sub>X<sub>88</sub>E<sub>65</sub>) using an ARES-G2 rheometer (Thermal Analysis Instruments, New Castle, DE) under nitrogen gas purge employing an 8 mm parallel plate geometry and a 0.5 mm gap. Frequency sweeps spanning 0.1 - 100 rad/s at a constant strain amplitude of 2% were conducted from 120 to 240 °C in 20 °C increments with 10 minutes between measurements for temperature equilibration. Master curves, referenced to 180 °C, were prepared using time-temperature superposition.

#### **Acknowledgments**

Funding for this work was provided by the Center for Sustainable Polymers, a National Science Foundation (NSF)-supported Center for Chemical Innovation (CHE-1413862). Parts of the work were carried out in the Characterization Facility, University of Minnesota, which receives partial

- support from the NSF through the MRSEC (Award Number DMR-2011401) and the NNCI
- 2 (Award Number ECCS-2025124) programs.

#### References

3

- 4 (1) Patel, K.; Chikkali, S. H.; Sivaram, S. Ultrahigh Molecular Weight Polyethylene: Catalysis,
- 5 Structure, Properties, Processing and Applications. *Prog. Polym. Sci.* **2020**, *109*, 101290.
- 6 https://doi.org/10.1016/j.progpolymsci.2020.101290.
- 7 (2) Billiet, S.; Trenor, S. R. 100th Anniversary of Macromolecular Science Viewpoint: Needs
- 8 for Plastics Packaging Circularity. ACS Macro Lett. 2020, 9 (9), 1376–1390.
- 9 https://doi.org/10.1021/acsmacrolett.0c00437.
- 10 (3) Thomas, L.; Ramachandra, M. Advanced Materials for Wind Turbine Blade- A Review.
- 11 Mater. Today: Proc. **2018**, 5 (1, Part 3), 2635–2640.
- 12 https://doi.org/10.1016/j.matpr.2018.01.043.
- 13 (4) Polyethylene market volume worldwide 2015-2029. Statista.
- https://www.statista.com/statistics/1245162/polyethylene-market-volume-worldwide/
- 15 (accessed 2023-01-12).
- 16 (5) Polypropylene global market volume 2015-2029. Statista.
- 17 https://www.statista.com/statistics/1245169/polypropylene-market-volume-worldwide/
- 18 (accessed 2023-01-12).
- 19 (6) Nakatani, J.; Maruyama, T.; Moriguchi, Y. Revealing the Intersectoral Material Flow of
- Plastic Containers and Packaging in Japan. Proc. Natl. Acad. Sci. U.S.A. 2020, 117 (33),
- 21 19844–19853. https://doi.org/10.1073/pnas.2001379117.
- 22 (7) Law, K. L.; Starr, N.; Siegler, T. R.; Jambeck, J. R.; Mallos, N. J.; Leonard, G. H. The United
- States' Contribution of Plastic Waste to Land and Ocean. Sci. Adv. 2020, 6 (44), eabd0288.
- 24 https://doi.org/10.1126/sciadv.abd0288.
- 25 (8) Peng, Y.; Wu, P.; Schartup, A. T.; Zhang, Y. Plastic Waste Release Caused by COVID-19
- and Its Fate in the Global Ocean. *Proc. Natl. Acad. Sci. U.S.A.* **2021**, *118* (47), e2111530118.
- 27 https://doi.org/10.1073/pnas.2111530118.
- 28 (9) US EPA, O. Advancing Sustainable Materials Management: 2018 Fact Sheet.
- 29 https://www.epa.gov/facts-and-figures-about-materials-waste-and-recycling/advancing-
- 30 sustainable-materials-management (accessed 2022-08-23).
- 31 (10) Mangold, H.; von Vacano, B. The Frontier of Plastics Recycling: Rethinking Waste as a
- Resource for High-Value Applications. *Macromol. Chem. Phys.* **2022**, *223* (13), 2100488.
- 33 https://doi.org/10.1002/macp.202100488.
- 34 (11) Garcia, J. M.; Robertson, M. L. The Future of Plastics Recycling. *Science* **2017**, *358* (6365),
- 35 870–872. https://doi.org/10.1126/science.aaq0324.
- 36 (12) Dai, L.; Ruan, R.; You, S.; Lei, H. Paths to Sustainable Plastic Waste Recycling. Science
- 37 **2022**, 377 (6609), 934–934. https://doi.org/10.1126/science.ade2221.

- 1 (13) Jehanno, C.; Alty, J. W.; Roosen, M.; De Meester, S.; Dove, A. P.; Chen, E. Y.-X.; Leibfarth, F. A.; Sardon, H. Critical Advances and Future Opportunities in Upcycling Commodity Polymers. *Nature* **2022**, *603* (7903), 803–814. https://doi.org/10.1038/s41586-021-04350-0.
- 4 (14) Xu, Z.; Pan, F.; Sun, M.; Xu, J.; Munyaneza, N. E.; Croft, Z. L.; Cai, G.; Liu, G. Cascade Degradation and Upcycling of Polystyrene Waste to High-Value Chemicals. *Proc. Natl. Acad. Sci. U.S.A.* **2022**, *119* (34), e2203346119. https://doi.org/10.1073/pnas.2203346119.
- 7 (15) Coates, G. W.; Getzler, Y. D. Y. L. Chemical Recycling to Monomer for an Ideal, Circular Polymer Economy. *Nat Rev Mater* **2020**, *5* (7), 501–516. https://doi.org/10.1038/s41578-020-0190-4.
- 10 (16) Schyns, Z. O. G.; Shaver, M. P. Mechanical Recycling of Packaging Plastics: A Review. 11 *Macromol. Rapid Commun.* **2021**, *42* (3), 2000415. https://doi.org/10.1002/marc.202000415.
- 12 (17) Yin, S.; Tuladhar, R.; Shi, F.; Shanks, R. A.; Combe, M.; Collister, T. Mechanical 13 Reprocessing of Polyolefin Waste: A Review. *Polym. Eng. Sci.* **2015**, *55* (12), 2899–2909. 14 https://doi.org/10.1002/pen.24182.
- 15 (18) Jubinville, D.; Esmizadeh, E.; Saikrishnan, S.; Tzoganakis, C.; Mekonnen, T. A
  16 Comprehensive Review of Global Production and Recycling Methods of Polyolefin (PO)
  17 Based Products and Their Post-Recycling Applications. *SM&T* **2020**, *25*, e00188.
  18 https://doi.org/10.1016/j.susmat.2020.e00188.
- 19 (19) Vogt, B. D.; Stokes, K. K.; Kumar, S. K. Why Is Recycling of Postconsumer Plastics so Challenging? *ACS Appl. Polym. Mater.* **2021**, *3* (9), 4325–4346. https://doi.org/10.1021/acsapm.1c00648.
- 22 (20) Graziano, A.; Jaffer, S.; Sain, M. on Modification Review Strategies 23 Polyethylene/Polypropylene Immiscible Thermoplastic Polymer Blends for Enhancing Their 24 Mechanical Behavior. J. Elastomers Plast. 2019, 51 (4),291–336. 25 https://doi.org/10.1177/0095244318783806.
- 26 (21) Teh, J. W.; Rudin, A.; Keung, J. C. A Review of Polyethylene–Polypropylene Blends and Their Compatibilization. *Adv. Polym. Technol.* **1994**, *13* (1), 1–23. https://doi.org/10.1002/adv.1994.060130101.
- 29 (22) Chaffin, K. A.; Knutsen, J. S.; Brant, P.; Bates, F. S. High-Strength Welds in Metallocene 30 Polypropylene/Polyethylene Laminates. *Science* **2000**, *288* (5474), 2187–2190. 31 https://doi.org/10.1126/science.288.5474.2187.
- 32 (23) Eagan, J. M.; Xu, J.; Di Girolamo, R.; Thurber, C. M.; Macosko, C. W.; LaPointe, A. M.; Bates, F. S.; Coates, G. W. Combining Polyethylene and Polypropylene: Enhanced Performance with PE/IPP Multiblock Polymers. *Science* **2017**, *355* (6327), 814–816. https://doi.org/10.1126/science.aah5744.
- 36 (24) Xu, J.; Eagan, J. M.; Kim, S.-S.; Pan, S.; Lee, B.; Klimovica, K.; Jin, K.; Lin, T.-W.; Howard, 37 M. J.; Ellison, C. J.; LaPointe, A. M.; Coates, G. W.; Bates, F. S. Compatibilization of 38 Isotactic Polypropylene (IPP) and High-Density Polyethylene (HDPE) with IPP-PE 39 Copolymers. Macromolecules 2018, 51 8585-8596. Multiblock (21),40 https://doi.org/10.1021/acs.macromol.8b01907.

- 1 (25) D'Orazio, L.; Greco, R.; Mancarella, C.; Martuscelli, E.; Ragosta, G.; Silvesrte, C. Effect of 2 the Addition of Ethylene-Propylene Random Copolymers on the Properties of High-Density 3 Polyethylene/Isotactic Polypropylene Blends: Part 1—Morphology and Impact Behavior of 4 Molded Samples. Polvm. Eng. Sci. 1982. 22 (9),536-544. https://doi.org/10.1002/pen.760220904. 5
- (26) D'Orazio, L.; Greco, R.; Martuscelli, E.; Ragosta, G. Effect of the Addition of EPM Copolymers on the Properties of High Density Polyethylene/Isotactic Polypropylene Blends:
   II. Morphology and Mechanical Properties of Extruded Samples. *Polym. Eng. Sci.* 1983, 23
   (9), 489–497. https://doi.org/10.1002/pen.760230903.
- 10 (27) Louizi, M.; Massardier, V.; Cassagnau, P. Contribution of High-Shear Processing to the Compatibilization of (PP/EPR)/PE Ternary Blends. *Macromol. Mater. Eng.* **2014**, *299* (6), 674–688. https://doi.org/10.1002/mame.201300268.
- 13 (28) Nedkov, T.; Lednický, F. Morphologies of Polyethylene–Ethylene/Propylene/Diene 14 Monomer Particles in Polypropylene-Rich Polyolefin Blends: Flake Structure. *J. Appl. Polym.* 15 *Sci.* **2003**, *90* (11), 3087–3092. https://doi.org/10.1002/app.13050.
- 16 (29) Hemmati, M.; Nazokdast, H.; Shariat Panahi, H. Study on Morphology of Ternary Polymer 17 Blends. I. Effects of Melt Viscosity and Interfacial Interaction. *J. Appl. Polym. Sci.* **2001**, *82* 18 (5), 1129–1137. https://doi.org/10.1002/app.1947.
- 19 (30) Lin, Y.; Yakovleva, V.; Chen, H.; Hiltner, A.; Baer, E. Comparison of Olefin Copolymers as Compatibilizers for Polypropylene and High-Density Polyethylene. *J. Appl. Polym. Sci.* **2009**, 21 *I13* (3), 1945–1952. https://doi.org/10.1002/app.30190.
- 22 (31) Lin, Y.; Marchand, G. R.; Hiltner, A.; Baer, E. Adhesion of Olefin Block Copolymers to 23 Polypropylene and High Density Polyethylene and Their Effectiveness as Compatibilizers in 24 Blends. *Polymer* **2011**, *52* (7), 1635–1644. https://doi.org/10.1016/j.polymer.2011.02.012.
- (32) Wolff, P.; Dickert, A.; Kretschmer, W. P.; Kempe, R. IPP/PE Multiblock Copolymers for
   Plastic Blend Recycling Synthesized by Coordinative Chain Transfer Polymerization.
   *Macromolecules* 2022, 55 (15), 6435–6442. https://doi.org/10.1021/acs.macromol.2c00709.
- 28 (33) Klimovica, K.; Pan, S.; Lin, T.-W.; Peng, X.; Ellison, C. J.; LaPointe, A. M.; Bates, F. S.; Coates, G. W. Compatibilization of IPP/HDPE Blends with PE-g-IPP Graft Copolymers.

  30 ACS Macro Lett. 2020, 9 (8), 1161–1166. https://doi.org/10.1021/acsmacrolett.0c00339.
- 31 (34) Singha, N. K.; Bhattacharjee, S.; Sivaram, S. Hydrogenation of Diene Elastomers, Their Properties and Applications: A Critical Review. *Rubber Chemistry and Technology* **1997**, *70* (3), 309–367. https://doi.org/10.5254/1.3538435.
- (35) Fetters, L. J.; Meyer, B. H.; McIntyre, D. The Effect of Diblock and Homopolymer Impurities
   on the Morphology of Triblock Polymers. *J. Appl. Polym. Sci.* 1972, *16* (8), 2079–2089.
   https://doi.org/10.1002/app.1972.070160819.
- 37 (36) Schulz, D. N.; Halasa, A. F. Anionic Polymerization Initiators Containing Protected Functional Groups. II. *J. Polym. Sci., Polym. Chem. Ed.* **1977**, *15* (10), 2401–2410. https://doi.org/10.1002/pol.1977.170151010.
- 40 (37) Cho, J. C.; Kim, K. H.; Kim, K. U.; Kwak, S.; Kim, J.; Jo, W. H.; Chun, M. S.; Lee, C. H.; Yeo, J. K.; Quirk, R. P. Microstructure Effect in the Coupling Reactions of Polymeric

- Organolithium Compounds Using Chlorosilanes. J. Polym. Sci., Part A: Polym. Chem. 1998,
- 2 36 (11), 1743–1753. https://doi.org/10.1002/(SICI)1099-0518(199808)36:11<1743::AID-POLA7>3.0.CO;2-S.
- 4 (38) Jose, S.; Aprem, A. S.; Francis, B.; Chandy, M. C.; Werner, P.; Alstaedt, V.; Thomas, S. Phase Morphology, Crystallisation Behaviour and Mechanical Properties of Isotactic Polypropylene/High Density Polyethylene Blends. *European Polymer Journal* **2004**, *40* (9), 2105–2115, https://doi.org/10.1016/j.eurpolymi.2004.02.026.
- 8 (39) Wignall, G. D.; Londono, J. D.; Lin, J. S.; Alamo, R. G.; Galante, M. J.; Mandelkern, L. Morphology of Blends of Linear and Long-Chain-Branched Polyethylenes in the Solid State:
  10 A Study by SANS, SAXS, and DSC. *Macromolecules* **1995**, *28* (9), 3156–3167.
  11 https://doi.org/10.1021/ma00113a018.
- 12 (40) Bates, F. S.; Fredrickson, G. H. Conformational Asymmetry and Polymer-Polymer 13 Thermodynamics. *Macromolecules* **1994**, 27 (4), 1065–1067. 14 https://doi.org/10.1021/ma00082a030.
- (41) Bates, F. S.; Schulz, M. F.; Rosedale, J. H.; Almdal, K. Correlation of Binary Polyolefin
   Phase Behavior with Statistical Segment Length Asymmetry. *Macromolecules* 1992, 25 (20),
   5547–5550. https://doi.org/10.1021/ma00046a070.
- 18 (42) Fredrickson, G. H.; Liu, A. J.; Bates, F. S. Entropic Corrections to the Flory-Huggins Theory 19 of Polymer Blends: Architectural and Conformational Effects. *Macromolecules* **1994**, *27* (9), 20 2503–2511. https://doi.org/10.1021/ma00087a019.
- 21 (43) Weimann, P. A.; Jones, T. D.; Hillmyer, M. A.; Bates, F. S.; Londono, J. D.; Melnichenko, 22 Y.; Wignall, G. D.; Almdal, K. Phase Behavior of Isotactic 23 Polypropylene-Poly(Ethylene/Ethylethylene) Random Copolymer Blends. *Macromolecules* **1997**, 30 (12), 3650–3657. https://doi.org/10.1021/ma961383h. 24
- (44) Chaffin, K. A.; Bates, F. S.; Brant, P.; Brown, G. M. Semicrystalline Blends of Polyethylene
   and Isotactic Polypropylene: Improving Mechanical Performance by Enhancing the
   Interfacial Structure. *J. Polym. Sci., Part B: Polym. Phys.* 2000, 38 (1), 108–121.
   https://doi.org/10.1002/(SICI)1099-0488(20000101)38:1<108::AID-POLB14>3.0.CO;2-9.
- 29 (45) Macosko, C. W.; Guégan, P.; Khandpur, A. K.; Nakayama, A.; Marechal, P.; Inoue, T. Compatibilizers for Melt Blending: Premade Block Copolymers. *Macromolecules* **1996**, *29* (17), 5590–5598. https://doi.org/10.1021/ma9602482.
- 32 (46) Lyu, S.; Jones, T. D.; Bates, F. S.; Macosko, C. W. Role of Block Copolymers on Suppression 33 of Droplet Coalescence. *Macromolecules* **2002**, *35* (20), 7845–7855. 34 https://doi.org/10.1021/ma020754t.
- 35 (47) Adedeji, A.; Lyu, S.; Macosko, C. W. Block Copolymers in Homopolymer Blends: Interface vs Micelles. *Macromolecules* **2001**, *34* (25), 8663–8668. https://doi.org/10.1021/ma001944b.
- 37 (48) Self, J. L.; Zervoudakis, A. J.; Peng, X.; Lenart, W. R.; Macosko, C. W.; Ellison, C. J. Linear, Graft, and Beyond: Multiblock Copolymers as Next-Generation Compatibilizers. *JACS Au* **2022**, *2* (2), 310–321. https://doi.org/10.1021/jacsau.1c00500.
- 40 (49) Eckstein, A.; Suhm, J.; Friedrich, C.; Maier, R.-D.; Sassmannshausen, J.; Bochmann, M.; Mülhaupt, R. Determination of Plateau Moduli and Entanglement Molecular Weights of

- Isotactic, Syndiotactic, and Atactic Polypropylenes Synthesized with Metallocene Catalysts. *Macromolecules* **1998**, *31* (4), 1335–1340. https://doi.org/10.1021/ma971270d.
- 3 (50) Galante, M. J.; Mandelkern, L.; Alamo, R. G. The Crystallization of Blends of Different 4 Types of Polyethylene: The Role of Crystallization Conditions. *Polymer* **1998**, *39* (21), 5105– 5119. https://doi.org/10.1016/S0032-3861(97)10162-8.
- (51) Zervoudakis, A. J.; Sample, C. S.; Peng, X.; Lake, D.; Hillmyer, M. A.; Ellison, C. J.
   Dihydroxy Polyethylene Additives for Compatibilization and Mechanical Recycling of Polyethylene Terephthalate/Polyethylene Mixed Plastic Waste. *ACS Macro Lett.* 2022, *11* (12), 1396–1402. https://doi.org/10.1021/acsmacrolett.2c00601.
- 10 (52) Nomura, K.; Peng, X.; Kim, H.; Jin, K.; Kim, H. J.; Bratton, A. F.; Bond, C. R.; Broman, A. E.; Miller, K. M.; Ellison, C. J. Multiblock Copolymers for Recycling Polyethylene–
  12 Poly(Ethylene Terephthalate) Mixed Waste. *ACS Appl. Mater. Interfaces* **2020**, *12* (8), 9726–
  13 9735. https://doi.org/10.1021/acsami.9b20242.
- 14 (53) Ndoni, S.; Papadakis, C. M.; Bates, F. S.; Almdal, K. Laboratory-scale Setup for Anionic Polymerization under Inert Atmosphere. *Rev. Sci. Instrum* **1995**, *66* (2), 1090–1095. https://doi.org/10.1063/1.1146052.
- 17 (54) Ertem, S. P.; Onuoha, C. E.; Wang, H.; Hillmyer, M. A.; Reineke, T. M.; Lodge, T. P.; Bates, F. S. Hydrogenolysis of Linear Low-Density Polyethylene during Heterogeneous Catalytic Hydrogen–Deuterium Exchange. *Macromolecules* **2020**, *53* (14), 6043–6055. https://doi.org/10.1021/acs.macromol.0c00696.
- (55) Jackson, C.; Chen, Y.-J.; Mays, J. W. Size Exclusion Chromatography with Multiple Detectors: Solution Properties of Linear Chains of Varying Flexibility in Tetrahydrofuran. *J. Appl. Polym. Sci.* 1996, 61 (5), 865–874. https://doi.org/10.1002/(SICI)1097-4628(19960801)61:5<865::AID-APP20>3.0.CO;2-V.